Exciton-Phonon Interactions in Strained Domes of Monolayer MoS2 Studied by Resonance Raman Spectroscopy

Jessica S. Lemos *, Elena Blundo, Antonio Polimeni, Marcos A. Pimenta, Ariete Righi *

Posted Date: 30 August 2023

doi: 10.20944/preprints202308.1981.v1

Keywords: MoS2 dome; Raman excitation profile; biaxial strain

Article

Exciton-Phonon Interactions in Strained Domes of Monolayer MoS_2 Studied by Resonance Raman Spectroscopy

Jessica S. Lemos[1,*], Elena Blundo[2], Antonio Polimeni[2], Marcos A. Pimenta[1,3] and Ariete Righi[1,*]

[1] Departamento de Física, Universidade Federal de Minas Gerais, Belo Horizonte, Minas Gerais, 31270-901, Brazil
[2] Dipartimento di Fisica, Sapienza Università di Roma, Roma, 00185, Italy
[3] Departamento de Física, Universidade Federal do Ouro Preto, Campus Universitário Morro do Cruzeiro, ICEB, Ouro Preto, Minas Gerais, 35400-000, Brazil
* Correspondence: righi@fisica.ufmg.br (A.R.); jsantoslemos@ufmg.br (J.S.L.)

Abstract: This work describes a resonance Raman study performed in domes of monolayer MoS_2 using 23 different laser excitation energies covering the visible and near-infrared (NIR) ranges. The multiple-excitation results allowed us to investigate the exciton-phonon interactions of different phonons (A_1', E' and LA) with different electronic and excitonic optical transitions in biaxially strained monolayer MoS_2. The analysis of the intensities of the two first-order peaks, A_1' and E', and the double-resonance 2LA Raman band as a function of the laser excitation furnished the values of the energies of the indirect gap and the excitonic transitions in the strained MoS_2 domes. It was noticed that the out-of-plane A_1' phonon mode is significantly enhanced only by the indirect gap I and the C exciton, whereas the in-plane E' mode is only enhanced by the C exciton of MoS_2 dome, revealing thus a weak interaction of these phonons with the A and B excitons in the strained MoS_2 domes. On the other hand, the 2LA Raman band is significantly enhanced at the indirect gap I transition and by the A (or B) exciton, but not enhanced by the C exciton, showing thus that the LA edge-phonons that participate in the double resonance process in MoS_2 have a weak interaction with the C exciton.

Keywords: MoS_2 dome; Raman excitation profile; biaxial strain

1. Introduction

Two-dimensional (2D) materials exhibit unique properties that depend on various factors, including the material's chemical composition, atomic arrangement, thickness, and interlayer interactions [1,2]. Modification of the intrinsic properties of crystalline materials is often necessary to achieve new fundamental effects or create favorable conditions for device fabrication. By carefully tuning these parameters, researchers can unlock new properties and behaviors in solid-state materials, leading to innovative technologies and scientific discoveries [2–4]. Recent studies have explored the effects of mechanical deformation and stress on the properties of 2D materials [5–9]. In particular, the ability of 2D materials to be easily strained is of great interest, as strain engineering can significantly impact their electronic and optical properties [8,10–16]. Indeed, many theoretical works have predicted that biaxial strain is particularly effective in tuning the band structure of transition metal dichalcogenides (TMDs) [17–22].

Atomically thin materials of the MoS_2-type family are particularly well-suited for studying the effects of mechanical deformation and stress because they can withstand extreme nonhomogeneous deformations before rupture [9,23–25]. The electronic and optical properties of MoS_2 monolayers are strongly coupled to the valley/spin/orbital degrees of freedom and the lattice structure, making them sensitive to mechanical deformation or stress [5,11,25–28]. To explore the effect of biaxial strain on TMDs, various methods have been developed, such as deposition on nanocones [29] or pillars [30] and epitaxial growth of superlattices [31]. In these methods, the strain obtained is typically around

Preprints (www.preprints.org) | NOT PEER-REVIEWED | Posted: 30 August 2023 doi:10.20944/preprints202308.1981.v1

1-2%. However, values of strain of 5% are reached at the center of MoS_2 monolayer domes that are investigated in this work [11,32].

In this letter, we present a resonant Raman spectroscopy study of MoS_2 dome sample using 23 different laser excitation energies in the NIR and visible ranges. Our measurements allowed us to obtain the Raman excitation profiles (REPs) of the first-order E' and A_1' Raman modes, as well as the REP of the second-order 2LA Raman band. Our results show that the three Raman bands are significantly enhanced at the indirect gap transition at 1.61 eV and by the C exciton at 2.72 eV, but the interaction of the first-order modes with the A and B excitons was shown to be very weak in the strained MoS_2 dome. It was also observed redshifts in the energies of the A and B excitons, in agreement with previous photoluminescence (PL) results [11,18,21,33], as well as in the energy of the C excitons, that was not yet reported in the literature. Our work provides important insights into the effects of biaxial strain on the excitonic and optical properties of 2D materials, which could have implications for the development of innovative technologies and scientific discoveries.

2. Materials and Methods

Figure 1(a) displays an optical image of a MoS_2 dome, created according to the procedure outlined by Tedeschi *et al.* [34] to generate isolated or conglomerates of semispherical nano- and micrometric domes. Raman maps were acquired using a Horiba LabRAM HR Evolution spectrometer equipped with a grating of 1800 lines/mm. A NIKON objective with a magnification of 100× and numerical aperture of 0.9 was used, and the laser energy of 2.34 eV was set to a power of 100 μW to prevent heating and bursting of the dome. In addition to this setup, another equipment was used, the HORIBA T64000 triple-monochromator spectrometer, using different laser sources (Ar-Kr, He-Ne, Ti-Shappire and solid-state lasers) to cover a wide range of excitation energies from 1.59 to 2.73 eV. An objective of 100× magnification and a laser power around 10 μW were used to avoid heating and bursting of the dome. Raman measurements were performed with linearly polarized lasers, but without an analyzer for the scattered light. All measurements were realized at room temperature with a backscattering configuration.

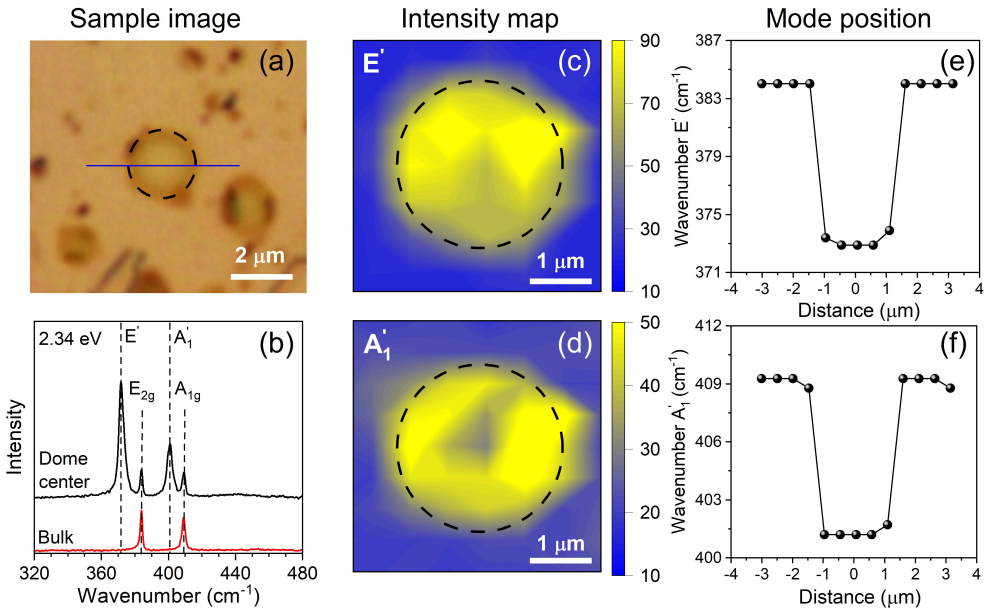

Figure 1. (a) Optical image of the sample. The dome edge is delimited by a black dashed line. (b) Raman spectra of the dome center (black) and of the MoS_2 bulk flake (red) acquired with excitation energy of 2.34 eV. (c) and (d) Intensity Raman maps of the first-order Raman modes E' and A'_1, respectively. (e) and (f) Positions of first-order Raman modes, E' and A'_1, measured along the blue line showed in Figure 1(a), respectively.

Preprints (www.preprints.org) | NOT PEER-REVIEWED | Posted: 30 August 2023 doi:10.20944/preprints202308.1981.v1

The photoluminescence measurements were conducted using a HORIBA T64000 triple-monochromator spectrometer in a single mode which was equipped with a grating of 300 lines/mm. The excitation was done with a VERDI laser that is an energy of 2.33 eV. A 100x magnification objective was employed, with the laser power set to approximately 100 μW. These measurements were performed at room temperature, employing a backscattering configuration.

3. Results

We began our study by characterizing the Raman modes of a selected dome. Figure 1 presents the optical image, the Raman spectra and intensity Raman maps acquired, and positions of A'_1 and E' modes from sample. The dashed circles around the dome delineate its edge. Figure 1(a) shows that the semispherical dome has a diameter of approximately (2.4 ± 0.1) μm. Figure 1(b) presents the Raman spectra recorded at the center of the dome (black line) and at the MoS_2 bulk substrate (red line) with 2.34 eV laser energy. The bulk's Raman spectrum exhibits two modes, E_{2g} and A_{1g}, located around 384 cm^{-1} and 409 cm^{-1}, respectively [35,36]. The Raman spectra at the dome's center exhibit four modes, where the two weaker peaks come from the bulk's substrate and the two more intense peaks, shifted to lower wavenumbers around 373 cm^{-1} and 402 cm^{-1}, are associated with the E' and $A_1{}'$ modes of the monolayer dome, respectively. In the literature, the positions of the E' and $A_1{}'$ modes in unstrained monolayer MoS_2 are 385 cm^{-1} and 404 cm^{-1}, respectively [36–38]. Therefore, the redshifts in the mode positions of the strained monolayer MoS_2 studied in this work with respect to the unstrained monolayer MoS_2 are 12 cm^{-1} and 2 cm^{-1} for the E' and $A_1{}'$ modes, respectively [38]. Previous studies have shown that the effect of the biaxial strain at the dome is more significant for the E' mode, with a displacement rate of 2.2 $cm^{-1}/\%$ [5]. According to this relation, the shift of 12 cm^{-1} observed in our work for the E' mode corresponds to a value of $\approx$ 5.5% of strain at the dome's center shown in Figure 1(a).

Figures 1(c)-(f) show the intensity maps and positions of the dome peaks acquired with a laser energy of 2.34 eV. The intensity maps of the E' and A'_1 Raman peaks indicate an increase in the modes intensities at the dome's region compared to the bulk spectra, as displayed in Figures 1(c) and 1(d), respectively. The positions of the E' and $A_1{}'$ Raman peaks at the monolayer dome's center are red-shifted by about 11 cm^{-1} and 7 cm^{-1}, respectively, when compared to the bulk's positions, as shown in Figures 1(e) and 1(f), respectively.

Figure 2(a) shows the Raman spectra recorded at the dome's center using five different laser excitation energies: 1.59 eV (780 nm), 1.68 eV (738 nm), 1.92 eV (646 nm), 2.38 eV (521 nm) and 2.73 eV (454 nm). The three dashed lines serve as guides to follow the positions of the in-plane E', the out-of-plane $A_1{}'$ and the 2LA modes. The Raman spectra of the bulk sample were subtracted from the spectra, so that it only displays the peaks of the dome's center. In addition to the first order-modes, we can observe the second-order 2LA Raman bands [39] centered around 440 cm^{-1}.

In the spectrum of the 1.59 eV excitation energy, we can observe an intense and sharp peak associated with the out-of-plane $A_1{}'$ mode and the broad 2LA band. Notice that the in-plane E' mode is absent in this spectrum. In the 1.68 eV excitation energy spectrum, the $A_1{}'$ mode is still the most intense, the 2LA band is observed and we can see the appearance of a broad band in the position of the E' mode. In the 1.92 eV excitation energy spectrum, we can observe that the broad 2LA band becomes the most intense, and the appearance of the E' mode is clearly observed. The broad band near the position of the E' mode is related to a double-resonance Raman process involving different valleys of MoS_2 [40]. By increasing the excitation energy, we can observe in the 2.38 eV excitation energy spectrum that the E' mode becomes as intense as the $A_1{}'$ mode, and the 2LA band is absent in the spectrum. In the highest 2.73 eV excitation energy spectrum, we see that the E' mode becomes more intense than the $A_1{}'$ mode.

Figure 2(b) shows the result of a multiple excitation energy Raman map at the MoS_2 dome's center obtained using different 23 laser lines with excitation energies ranging from 1.59 to 2.73 eV. The peak intensities in these figures were normalized by the quartz intensity, and are represented by the color

Preprints (www.preprints.org) | NOT PEER-REVIEWED | Posted: 30 August 2023 doi:10.20944/preprints202308.1981.v1

bar. The energies of the incident photon are on the vertical scale, and the horizontal scale represents the Raman shifts. The blank gap in excitation energies between 1.69 and 1.88 eV in Figure 2(b) is a region where we do not have available laser lines.

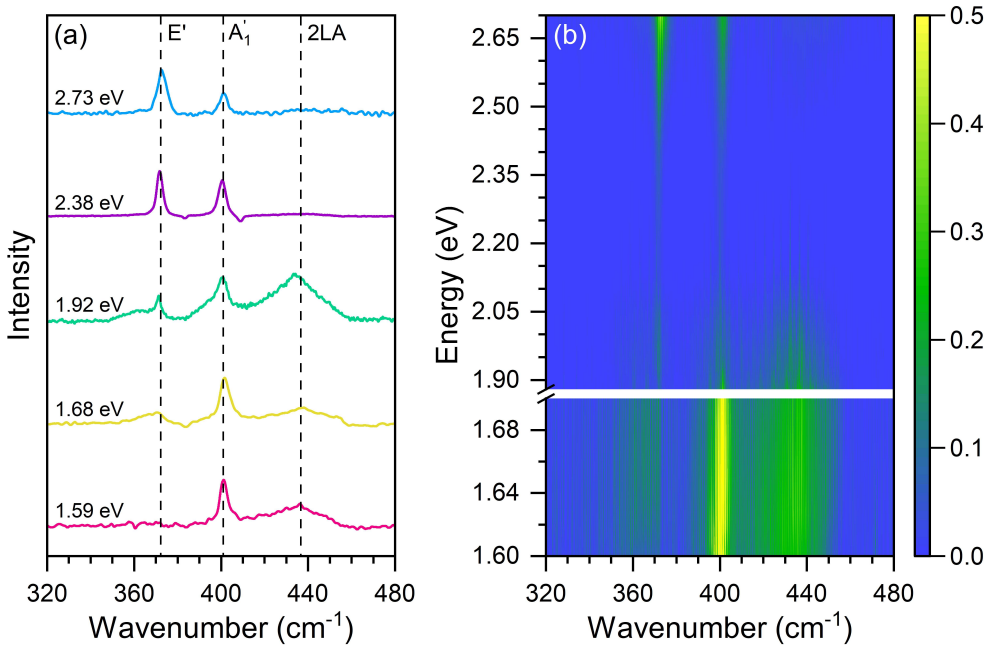

Figure 2. (a) Raman spectra of the MoS_2 dome center with five excitation energies: 1.59 eV (pink line), 1.68 eV (yellow line), 1.92 eV (green line), 2.38 eV (purple line) and 2.73 eV (blue line). (b) Raman map of the dome center with twenty-three laser lines with photon energies in the Vis-NIR range.

Figure 3 shows the Raman excitation profiles (REPs) of the A_1', E′ and 2LA bands, that is, the intensity of each feature as a function of the laser excitation energy. We will discuss separately the results of the first-order modes and the 2LA band. The REPs of the first-order A_1' (open red squares) and E′ (dark blue triangles) modes are shown in Figure 3, and the lines represent the best fits of the experimental data considering the equation for Raman intensity as a function of the laser energy E_L for a first-order (one-phonon) process given by [40]:

$$I^k(E_L) = \sum_i \left| \frac{M_{\text{el-rad}} . M_{ex-ph}^{(i)-(k)} . M_{\text{el-rad}}}{(E_L - E_{ex}^i - i\gamma^i)(E_L - E_{ph}^k - E_{ex}^i - i\gamma^i)} \right|^2, \quad (1)$$

where the index i denotes the electronic or excitonic transition, the index k denotes the two phonons (A_1' or E′) and the three terms in the numerator represent the matrix elements of the electron-radiation (absorption of the incident photon), exciton-phonon, and electron-radiation (emission of the scattered photon) interactions, respectively. The two terms in the denominator give rise to the resonant enhancement of the Raman peaks when the incident or scattered photon energies match the exciton energy. The damping constant γ^i is related to the finite lifetime of the exciton i involved in the Raman process, E_{ex}^i is the energy of exciton i and E_{ph}^k is the energy of phonon k.

Preprints (www.preprints.org) | NOT PEER-REVIEWED | Posted: 30 August 2023 doi:10.20944/preprints202308.1981.v1

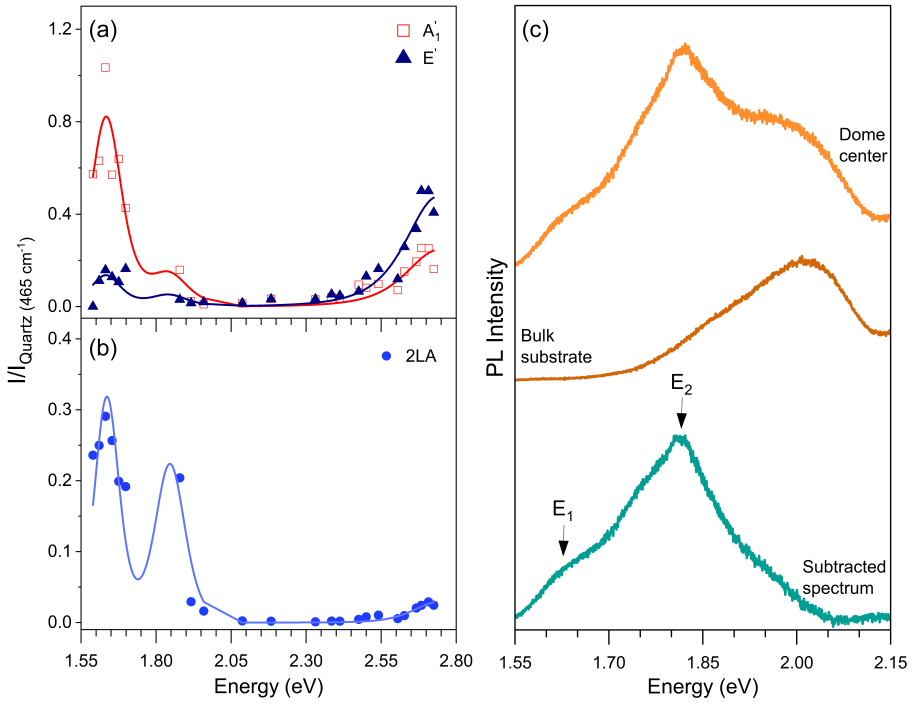

Figure 3. (a) Raman excitation profile (REP) of the first-order Raman modes $E^{'}$ (dark blue triangles) and $A^{'}_1$ (open red squares). (b) REP of the 2LA Raman mode (blue circles). (c) Photoluminescence spectrum acquired at the dome center (orange), MoS_2 bulk substrate (brown) and subtracted spectrum (green) resulting from the difference between the dome center and bulk spectra. The arrows indicate the position of the energies obtained in the REP.

Figure 3(a) clearly shows three resonances in the REPs in the investigated range of energies. Notice that the out-of-plane $A^{'}_1$ mode is enhanced by the three resonances, whereas the in-plane $E^{'}$ mode is weakly enhanced at lower energy resonance, but is more intense than the $A_1{}^{'}$ mode at higher energies in Figure 3(a).

In the fitting process, the same set of parameters of the excitons (energies and damping constants) was used to fit the REPs of the different phonon modes. Table 1 shows the fitting parameters (exciton energies and damping constants) that provide the best fit of the experimental REP data and are represented by the solid curves in Figure 3(a). The values for the first resonance (E_1) are more accurate since we have more experimental data in this energy region. The lack of experimental points in the range 1.69-1.88 eV prevented us to measure with accuracy the second resonance (E_2) energy and linewidth. The accuracy in the value of the third resonance energy (E_3) is also poor since we do not have experimental points above 2.8 eV.

We will now discuss the resonance Raman behavior of the 2LA band, that comes from a second-order phonon process involving two phonons of the longitudinal acoustic (LA) branch near the Brillouin zone edge (K and M points)[39]. Figure 3(b) shows the REP of the 2LA mode, where the blue circles represent the experimental data and the curves represent the best fit considering the expression for the intensity of a second-order Raman process as a function of the laser energy E_L given by following expression[39]:

$$I^{2LA}(E_L) = \sum_i \left| \frac{M_{\text{el-rad}} . M^{(i)-LA}_{ex-ph} . M^{(i)-LA}_{ex-ph} . M_{\text{el-rad}}}{(E_L - E^i_{ex} - 2E^{LA}_{ph} - i\gamma^i)(E_L - E^i_{ex} - E^{LA}_{ph} - i\gamma^i)(E_L - E_{ex} - i\gamma^i)} \right|^2 , \quad (2)$$

where the two middle terms in the numerator of Eq.2 represent the exciton-phonon interactions involving two phonons with opposite momenta. The denominator shows three terms that gives the

Preprints (www.preprints.org) | NOT PEER-REVIEWED | Posted: 30 August 2023 doi:10.20944/preprints202308.1981.v1

resonances of the incident photon and the scattered photon with one and by two phonons. The REP of the 2LA Raman band shown in Figure 3(b) was fitted using the same energy values of the E_1, E_2 and E_3 shown in Table 1. We can observe that the 2LA band is significantly enhanced at lower energies (E_1 and E_2) but only very weakly enhanced at the higher energy resonance (E_3).

Table 1. Energies and damping constants of the observed resonances in the Raman excitation profile in strained MoS_2.

Resonance	Energy (eV)	Damping (eV)
E_1	1.61 ± 0.01	0.09
E_2	1.82 ± 0.05	0.11
E_3	2.72 ± 0.05	0.19

Figure 3(c) shows the photoluminescence spectra recorded at the dome center (upper spectrum), at the MoS_2 bulk substrate (middle spectrum), and the subtraction between the two first ones in the bottom, where we can only observe the contribution of the strained MoS_2 single layer.

4. Discussion

Let us now discuss the physical origin of the three resonances E_1, E_2 and E_3 observed in the resonace Raman results. For the first-order $A_1^{'}$ and $E^{'}$, we have observed that the out-of-plane $A_1^{'}$ mode is strongly enhanced at E_1 and E_3, whereas the in-plane $E^{'}$ is only strongly enhanced at the higher resonance energy E_3. On the other hand, the second-order 2LA band is significantly enhanced at E_1 and E_2 and practically not observed at E_3.

The highest resonance energy E_3 can be attributed to exciton C of MoS_2, whose energy in unstrained monolayer MoS_2 is around 2.9 eV as observed by resonance Raman spectroscopy [41], and is far isolated from the other lower energy excitons in the optical spectrum. The observed value of the C-exciton energy at 2.72 eV allows us to conclude that is redshifted by about 0.18 eV in the strained domes with respect to the unstrained MoS_2 monolayer, similarly to the case of the energies of A and B excitons in the strained MoS_2 domes. Interestingly, the 2LA band is only very weakly enhanced at higher energies, revealing thus a weak interaction of the zone-edge LA phonons with the C exciton.

In order to assign the E_1 and E_2 resonances in the REP we acquired the photoluminescence (PL) spectrum on the same dome, whose REP curves are displayed in Figure 3(a,b). The topmost trace in Figure 3 (c) is the PL spectrum recorded with the laser spot centred on the top of the MoS_2 dome. The emission from the MoS_2 substrate (or bulk) adjacent to the dome is given by the middle trace in Figure 3 (c). Finally, the bottommost trace in Figure 3 (c) is obtained by subtracting the bulk contribution from the spectrum recorded on the dome. It must be emphasized that the spectrum intensities were not corrected by the spectral response of the spectrometer (detector and gratings), and the intensities at lower energies are underestimated. Nevertheless, in the PL spectrum two clear resonances are observed. The latter match very well the E_1 and E_2 REP resonances, which are indicated by the arrows in the lower part of Figure 3 (c).

Previous PL studies on strained MoS_2 domes similar to those investigated here showed the presence of two main contributions to the emission spectrum acquired close to the top of the dome [11] like in the present case. The lower and higher energy resonances in the PL spectrum were attributed to the indirect and direct exciton, respectively. As a matter of fact, for sufficiently high strain values (typically greater than 2%) the maximum of the valence band (VB) of the MoS_2 monolayer undergoes a transition from K to Γ (the same occurs in WS_2 and WSe_2 monolayers as reported in Ref. [11]). At the same time, the minimum of the conduction band (CB) at K moves at lower energy while remaining the lowest state of the CB. Consequently, the exciton transition with lowest energy becomes indirect in character (Γ_{VB}-K_{CB}), while the direct exciton transition (K_{VB}-K_{CB}) is at higher energy. It should be noted though that when the direct and indirect excitons are resonant they hybridise and their direct vs indirect character is smeared out. In particular, the indirect exciton may gain sufficiently

oscillator strength and become bright despite its k-space indirect character. Recently, evidence of exciton hybridisation was also observed in the strain dependence of the exciton magnetic moment in WS_2 domes [13]. By comparing the PL difference spectrum in Fig. 3 (c) with the results on MoS_2 domes reported in Ref. [11], we may attribute the E_1 resonance in the REP to the indirect exciton and the E_2 resonance to the direct exciton. Indeed, in Ref. [11], it was observed that the indirect exciton energy ranges between 1.65 eV and 1.62 eV depending on the position on the dome, in agreement with the E_1 resonance. The direct exciton was found to vary from 1.75 eV to 1.78 eV for increasing strain that suggests the E_2 resonance (E_2=1.82 $\pm$ 0.05 eV) being associated to the direct (or A) exciton state. Nevertheless, due to the large energy uncertainty of E_2 and its low spectral weight, we cannot exclude a possible contribution from the B exciton.

Finally, the different relative weight of the indirect (corresponding to E_1) and direct (corresponding to E_2) excitons in the PL spectra and in the REP curves probably comes from the exciton-phonon (or electron-phonon) interaction. The PL process involves two optical transitions and the Raman process involves not only the two optical transitions, but also the exciton-phonon intereaction, whose matrix element is given by the middle term in the numerator of Eq. 1, which is specific for each exciton *i* and phonon *k*.

5. Conclusions

In conclusion, this study presents a resonance Raman analysis of the first-order modes and of the the double-resonance 2LA band in a dome of strained monolayer MoS_2, using 23 different laser excitation energies in the range of 1.59 to 2.73 eV. It was observed that the Raman features are enhanced by three resonance energies, E_1, E_2, and E_3 at respectively 1.61 eV, 1.82 eV and 2.72 eV. It was observed that the out-of-plane $A_1^{'}$ mode is significantly enhanced by the first and the third resonances (E_1 and E_3) while the in-plane $E^{'}$ mode was only significantly enhanced at E_3. The 2LA band, that comes from a double-resonance Raman process involving two phonons, exhibited a different resonance behavior, since it was strongly enhanced at the two first resonances E_1 and E_2 and practically not observed at E_3. Our analysis allowed us to ascribe the third resonance to the C exciton of MoS_2. On the other hand, the high strain values (about 5%) that can be reached in the MoS_2 domes led to a direct-to-indirect band gap transition with the indirect exciton at lower energy than the direct (or A) exciton. As a matter of fact, the comparison between the strain-dependent PL spectra and the the REP curves indicated that the first and second resonances are consistent with the indirect and direct exciton, respectively. Our results show that the exciton phonon coupling involving the out-of-plane $A_1^{'}$ and the in-plane $E^{'}$ modes with the A exciton is small in strained MoS_2. On the other hand, the enhancement of the first-order modes by the C exciton, specially strong for the $E^{'}$ mode, reveals a strong exciton-phonon coupling in this case. The second order 2LA band exhibited a difference resonance behavior, since it is was significantly enhanced at the lower energy resonaces but practically not observed when the excitation energy matches the exciton C, revealing thus the selective exciton-phonon interaction for the double-resonance Raman process of MoS_2-type materials. These findings provide valuable insights into the behavior of MoS_2 under strain and its potential use in developing strain-based devices and contributes to the existing knowledge of MoS_2 physical properties.

Author Contributions: Sample Preparation, E.B. and A.P.; Raman and PL measurements, J.S.L; Project idealization and guidance, M.A.P, A.P. and A.R; Paper writing, J.S.L, M.A.P and A.R..All authors have contributed to data analysis and writing of the paper. All authors have read and agreed on the final version of the manuscript.

Funding: We gratefully acknowledge the financial support provided by the following Brazilian institutions: Instituto Nacional de Ciência e Tecnologia (INCT) em Nanomateriais de Carbono, Financiadora de Estudos e Projetos (FINEP), Coordenação de Aperfeiçoamento de Pessoal de Nível Superior (CAPES), Conselho Nacional de Desenvolvimento Científico e Tecnológico (CNPq), and Fundação de Amparo à Pesquisa do Estado de Minas Gerais (FAPEMIG). Without their support, this work would not have been possible. This project was partly funded within the QuantERA II Programme that has received funding from the European Union's Horizon 2020 research and innovation programme under Grant Agreement No 101017733, and with funding organisations Ministero dell'Universitá e della Ricerca (MUR) and Consiglio Nazionale delle Ricerche (CNR). We acknowledge financial support from the PNRR MUR project PE0000023-NQSTI.

Institutional Review Board Statement: Not applicable.

Informed Consent Statement: Not applicable.

Data Availability Statement: Not applicable.

Acknowledgments: Not applicable.

Conflicts of Interest: The authors declare no conflict of interest.

References

1. Hess, P. Bonding, structure, and mechanical stability of 2D materials: the predictive power of the periodic table. *Nanoscale Horiz.* **2021**, *6*, 856-892. [https://doi.org/10.1039/D1NH00113B]
2. Li, X.; Tao, L.; Chen, Z.; Fang, H.; Li, X.; Wang, X.; Xu, J.-B.; Zhu, H. Graphene and related two-dimensional materials: Structure-property relationships for electronics and optoelectronics. *Applied Physics Reviews* **2017**, *4*, 021306. https://doi.org/10.1063/1.4983646]
3. Geim, A.; Grigorieva, I. Van der Waals heterostructures. *Nature* **2013**, *499*, 419–425. [https://doi.org/10.1038/s43586-022-00139-1]
4. Butler, S. Z.; Hollen, S. M.; Cao, L.; Cui, Y.; Gupta, J. A.; Gutiérrez, H. R.; Heinz, T. F.; Hong, S. S.; Huang, J.; Ismach, A. F.; Johnston-Halperin, E.; Kuno, M.; Plashnitsa, V. V.; Robinson, R. D.; Ruoff, R. S.; Salahuddin, S.; Shan, J.; Shi, L.; Spencer, M. G.; Terrones, M.; Windl, W.; Goldberger, J. E. Progress, Challenges, and Opportunities in Two-Dimensional Materials Beyond Graphene. *ACS Nano* **2013**, *7*, 2898-2926. [https://doi.org/10.1021/nn400280c]
5. Blundo, E.; Cappelluti, E.; Felici, M.; Pettinari, G.; Polimeni, A. Strain-tuning of the electronic, optical, and vibrational properties of two-dimensional crystals. *Applied Physics Reviews* **2021**, *8*, 021318. [https://doi.org/10.1063/5.0037852]
6. Yang, S.; Chen, Y.; Jiang, C. Strain engineering of two-dimensional materials: Methods, properties, and applications. *InfoMat* **2021**, *3*, 397– 420. [https://doi.org/10.1002/inf2.12177]
7. Dai, Z.; Liu, L.; Zhang, Z. Strain Engineering of 2D Materials: Issues and Opportunities at the Interface. *Advanced Materials* **2019**, *31*, 1805417. [https://doi.org/10.1002/adma.201805417]
8. Roldán, R.; Castellanos-Gomez, A.; Cappelluti, E.; Guinea, F. Strain engineering in semiconducting two-dimensional crystals. *Journal of Physics: Condensed Matter* **2015**, *27*, 313201. [https://dx.doi.org/10.1088/0953-8984/27/31/313201]
9. Di Giorgio, C.; Blundo, E.; Pettinari, G.; Felici, M.; Bobba, F.; Polimeni, A. Mechanical, Elastic, and Adhesive Properties of Two-Dimensional Materials: From Straining Techniques to State-of-the-Art Local Probe Measurements. *Advanced Materials Interfaces* **2022**, *9*, 2102220. [https://doi.org/10.1002/admi.202102220]
10. Guinea, F.; Katsnelson, M.; Geim, A. Energy gaps ; a zero-field quantum Hall effect in graphene by strain engineering. *Nature Physics* **2010**, *6*, 30–33. [https://doi.org/10.1038/nphys1420]
11. Blundo, E.; Felici, M.; Yildirim, T.; Pettinari, G.; Tedeschi, D.; Miriametro, A.; Liu,B.; Ma, W.; Lu, Y.; Polimeni, A. Evidence of the direct-to-indirect band gap transition in strained two-dimensional WS_2, MoS_2 and WSe_2. *Physical Review Research* **2020**, *2*, 012024. [https://doi.org/10.1103/PhysRevResearch.2.012024]
12. Frisenda, R.; Drüppel, M.; Schmidt, R.; Michaelis de Vasconcellos, S.; Perez de Lara, D.; Bratschitsch, R.; Rohlfing, M.; Castellanos-Gomez, A. Biaxial strain tuning of the optical properties of single-layer transition metal dichalcogenides. *npj 2D Materials and Applications* **2017**, *1*, 10. [https://doi.org/10.1038/s41699-017-0013-7]
13. Blundo, E.; Faria Junior, P. E.; Surrente, A.; Pettinari, G.; Prosnikov, M. A.; Olkowska-Pucko, K.; Zollner, K.; Woźniak, T.; Chaves, A.; Kazimierczuk, T.; Felici, M.; Babiński, A.; Molas, M. R.; Christianen, P. C. M.; Fabian, J.; Polimeni, A. Strain-Induced Exciton Hybridization in WS_2 Monolayers Unveiled by Zeeman-Splitting

Measurements. *Physical Review Letters* **2022**, *129*, 067402.
[https://doi.org/10.1103/PhysRevLett.129.067402]

14. Li, F.; Shen, T.; Xu, L.; Hu, C.; Qi, J. Strain Improving the Performance of a Flexible Monolayer MoS2 Photodetector. *Advanced Electronic Materials* **2019**, *5*, 1900803.
[https://doi.org/10.1002/aelm.201900803]
15. Datye, I. M.; Daus, A.; Grady, R. W.; Brenner, K.; Vaziri, S.; Pop, E. Strain-Enhanced Mobility of Monolayer MoS_2. *Nano Letters* **2022**, *22*, 8052-8059.
[https://doi.org/10.1021/acs.nanolett.2c01707]
16. He, K.; Poole, C.; Mak, K. F.; Shan, J. Experimental Demonstration of Continuous Electronic Structure Tuning via Strain in Atomically Thin MoS_2. *Nano Letters* **2013**, *13*, 2931-2936.
[https://doi.org/10.1021/nl4013166]
17. Scalise, E.; Houssa, M.; Pourtois, G.; Afanas'ev, V.; Stesmans, A. Strain-induced semiconductor to metal transition in the two-dimensional honeycomb structure of MoS_2. *Nano Research* **2012**, *5*, 43-48.
[https://doi.org/10.1007/s12274-011-0183-0]
18. Johari, P.; Shenoy, V. B. Tuning the Electronic Properties of Semiconducting Transition Metal Dichalcogenides by Applying Mechanical Strains. *ACS Nano* **2012**, *6*, 5449-5456.
[https://doi.org/10.1021/nn301320r]
19. Guzman, D. M.; Strachan, A. Role of strain on electronic and mechanical response of semiconducting transition-metal dichalcogenide monolayers: An ab-initio study. *Journal of Applied Physics* **2014**, *115*, 243701.
[https://doi.org/10.1063/1.4883995]
20. Scalise, E.; Houssa, M.; Pourtois, G.; Afanasev, V.V.; Stesmans, A. First-principles study of strained 2D MoS_2. *Physica E: Low-dimensional Systems and Nanostructures* **2014**, *56*, 416-421.
[https://doi.org/10.1016/j.physe.2012.07.029]
21. Nguyen, C. V.; Hieu, N. N. Effect of biaxial strain and external electric field on electronic properties of MoS_2 monolayer: A first-principle study. *Chemical Physics* **2016**, *468*, 9-14.
[https://doi.org/10.1016/j.chemphys.2016.01.009]
22. Zollner, K.; Junior, P. E. F.; Fabian, J. Strain-tunable orbital, spin-orbit, and optical properties of monolayer transition-metal dichalcogenides. *Physical Review B* **2019**, *100*, 195126.
[https://doi.org/10.1103/PhysRevB.100.195126]
23. Lee, C.; Wei, X.; Kysar, J. W.; Hone, J. Measurement of the Elastic Properties and Intrinsic Strength of Monolayer Graphene. *Science* **2008**, *321*,385-388.
[https://www.science.org/doi/abs/10.1126/science.1157996]
24. Bertolazzi, S.; Brivio, J.; Kis, A. Stretching and Breaking of Ultrathin MoS_2. *ACS Nano* **2011**, *5*, 9703-9709.
[https://doi.org/10.1021/nn203879f]
25. Deng, S.; Sumant, A. V.; Berry, V. Strain engineering in two-dimensional nanomaterials beyond graphene. *Nano Today* **2018**, *22*, 14-35.
[https://doi.org/10.1016/j.nantod.2018.07.001]
26. Xiao, D.; Liu, G.-B.; Feng, W.; Xu, X.; Yao, W. Coupled Spin and Valley Physics in Monolayers of MoS_2 and Other Group-VI Dichalcogenides. *Physical Review Letters* **2012**, *108*, 196802.
[https://doi.org/10.1103/PhysRevLett.108.196802]
27. Amorim, B.; Cortijo, A.; de Juan, F.; Grushin, A. G.; Guinea, F.; Gutiérrez-Rubio, A.; Ochoa, H.; Parente, V.; Roldán, R.; San-Jose, P.; Schiefele, J.; Sturla, M.; Vozmediano, M. A. H. Novel effects of strains in graphene and other two dimensional materials. *Physics Reports* **2016**, *617*, 1-54.
[https://doi.org/10.1016/j.physrep.2015.12.006]
28. Lloyd, D.; Liu, X.; Christopher, J. W.; Cantley, L.; Wadehra, A.; Kim, B. L.; Goldberg, B. B.; Swan, A. K.; Bunch, J. S. Band Gap Engineering with Ultralarge Biaxial Strains in Suspended Monolayer MoS_2. *Nano Letters* **2016**, *16*, 5836-5841.
[https://doi.org/10.1021/acs.nanolett.6b02615] - Lloyd, D.; Liu, X.; Christopher, J. W.; Cantley, L.; Wadehra, A.; Kim, B. L.; Goldberg, B. B.; Swan, A. K.; Bunch, J. S. Correction to Band Gap Engineering with Ultralarge Biaxial Strains in Suspended Monolayer MoS_2. *Nano Letters* **2019**, *19*, 7548-7548.
[https://doi.org/10.1021/acs.nanolett.9b03591]
29. Li, H.; Tsai, C.; Koh, A. L.; Cai, L.; Contryman, A. W.; Fragapane, A. H.; Zhao, J.; Han, H. S.; Manoharan, H. C.; Abild-Pedersen, F.; Nørskov, J. K.; Zheng, X. Activating and optimizing MoS_2 basal planes for hydrogen

evolution through the formation of strained sulphur vacancies. *Nature Materials* **2016**, *15*, 48-53. [https://doi.org/10.1038/nmat4465]

30. Chaste, J.; Missaoui, A.; Huang, S.; Henck, H.; Ben Aziza, Z.; Ferlazzo, L.; Naylor, C.; Balan, A.; Johnson, A. T. C. Jr.; Braive, R.; Ouerghi, A. Intrinsic Properties of Suspended MoS_2 on SiO_2/Si Pillar Arrays for Nanomechanics and Optics. *ACS Nano* **2018**, *12*, 3235-3242. [https://doi.org/10.1021/acsnano.7b07689]

31. Xie, S.; Tu, L.; Han, Y.; Huang, L.; Kang, K.; Lao, K. U.; Poddar, P.; Park, C.; Muller, D. A.; Distasio, R. A.; Park, J. Coherent, atomically thin transition-metal dichalcogenide superlattices with engineered strain. *Science* **2018**, *359*, 1131-1136.
[https://doi.org/10.1126/science.aao5360]
32. Blundo, E.; Di Giorgio, C.; Pettinari, G.; Yildirim, T.; Felici, M.; Lu, Y.; Bobba, F.; Polimeni, A. Engineered Creation of Periodic Giant, Nonuniform Strains in MoS_2 Monolayers. *Advanced Materials Interfaces* **2020**, *7*, 2000621.
[https://doi.org/10.1002/admi.202000621]
33. Conley, H. J.; Wang, B.; Ziegler, J. I.; Haglund, R. F. Jr.; Pantelides, S. T.; Bolotin, K. I. Bandgap Engineering of Strained Monolayer and Bilayer MoS_2. *Nano Letters* **2013**, *13*, 3626-3630.
[https://doi.org/10.1021/nl4014748]
34. Tedeschi, D.; Blundo, E.; Felici, M.; Pettinari, G.; Liu, B.; Yildrim, T.; Petroni, E.; Zhang, C.; Zhu, Y.; Sennato, S.; Lu, Y.; Polimeni, A. Controlled Micro/Nanodome Formation in Proton-Irradiated Bulk Transition-Metal Dichalcogenides. *Advanced Materials* **2019**, *31*, 1903795.
[https://doi.org/10.1002/adma.201903795]
35. Pimenta, M. A.; del Corro, E.; Carvalho, B. R.; Fantini, C.; Malard, L. M. Comparative Study of Raman Spectroscopy in Graphene and MoS2-type Transition Metal Dichalcogenides. *Accounts of Chemical Research* **2015**, *48*, 41-47.
[https://doi.org/10.1021/ar500280m]
36. Zhang, X.; Qiao, X.-F.; Shi, W.; Wu, J.-B.; Jiang, D.-S.; Tan, P.-H. Phonon and Raman scattering of two-dimensional transition metal dichalcogenides from monolayer, multilayer to bulk material. *Chemical Society Reviews* **2015**, *44*, 2757-2785.
[https://doi.org/10.1039/C4CS00282B]
37. Li, H.; Zhang, Q.; Yap, C.C.R.; Tay, B.K.; Edwin, T.H.T.; Olivier, A.; Baillargeat, D. From Bulk to Monolayer MoS_2: Evolution of Raman Scattering. *Advanced Functional Materials* **2012**, *22*, 1385-1390.
[https://doi.org/10.1002/adfm.201102111]
38. R Saito, R.; Tatsumi, Y.; Huang, S.; Ling, X.; Dresselhaus, M.S. Raman spectroscopy of transition metal dichalcogenides. *Journal of Physics: Condensed Matter* **2016**, *28*, 353002.
[https://dx.doi.org/10.1088/0953-8984/28/35/353002]
39. Carvalho, B. R.; Wang, Y.; Mignuzzi, S.; Roy, D.; Terrones, M.; Fantini, C.; Crespi, V. H.; Malard, L. M.; Pimenta, M. A. Intervalley scattering by acoustic phonons in two-dimensional MoS_2 revealed by double-resonance Raman spectroscopy. *Nature Communications* **2017**, *8*, 14670.
[https://doi.org/10.1038/ncomms14670]
40. Carvalho, B. R.; Malard, L. M.; Alves, J. M.; Fantini, C.; Pimenta, M. A. Symmetry-Dependent Exciton-Phonon Coupling in 2D and Bulk MoS_2 Observed by Resonance Raman Scattering. *Physical Review Letters* **2015**, *114*, 136403.
[https://link.aps.org/doi/10.1103/PhysRevLett.114.136403]
41. Carvalho, B. R.; Malard, L. M.; Alves, J. M.; Fantini, C.; Pimenta, M. A. Erratum: Symmetry-Dependent Exciton-Phonon Coupling in 2D and Bulk MoS_2 Observed by Resonance Raman Scattering [Phys. Rev. Lett. 114, 136403 (2015)]. *Physical Review Letters* **2016**, *116*, 089904.
[https://link.aps.org/doi/10.1103/PhysRevLett.116.089904]